2023 IEEE International Conference on Robotics and Automation (ICRA 2023)
May 29 - June 2, 2023. London, UK

Anchoring Sagittal Plane Templates in a Spatial Quadruped

Timothy Greco and Daniel E. Koditschek

Abstract— **This paper introduces a new controller that stabilizes the motion of a spatial quadruped around sagittal-plane templates. It enables highly dynamic gaits and transitional maneuvers formed from parallel and sequential compositions of such planar templates in settings that require significant out-of-plane reactivity. The controller admits formal guarantees of stability with some modest assumptions. Experimental results validate the reliable execution of those planar template-based maneuvers, even in the face of large lateral, yaw, and roll incurring disturbances. This spatial anchor, fixed in parallel composition with a variety of different parallel and sequential compositions of sagittal plane templates, illustrates the robust portability of provably interoperable modular control components across a variety of hardware platforms and behaviors.**

I. Introduction

Animals exemplify the versatility of legged locomotion. They can pick their way through cluttered debris, run with agility, and use objects in their environment to increase their mobility. These behaviors have inspired the design and control of legged robots for decades. Robots like RHex [1] and ANYmal [2] have demonstrated robust traversal of unstructured natural terrain, and the widespread adoption and success of legged robots in DARPA's SubT challenge [3] testifies to their practical benefits. Substantial recent advances on these problems focus on finding suitable footholds [4] and learning to react to unexpected disturbances [2], [5], increasing the robustness of steady-state walking gaits in which the torso maintains nearly constant velocity.

Dynamic and highly energetic locomotion presents additional challenges for legged robots, as greater momentum requires the robot's movements to be faster, stronger, and more precise [6]. Learned controllers have achieved some high-speed locomotion at more than 8 body lengths per second [7], and some low-speed behaviors that interact with obstacles [8], but dynamic tasks like leaping have been restricted to simulation [9], [10]. Another paradigm for highly dynamic maneuvers uses model-predictive control (MPC) to calculate feasible body trajectories and desired ground-reaction forces [11]–[13]. The computational intensity of MPC often limits it to lower control rates than are suitable for legged robotics, so it is common to compose MPC with a whole-body controller (WBC) that calculates the necessary motor torques to either track the resulting trajectory [14] or produce the desired ground-reaction forces [13]. The MPC controller receives a goal trajectory either from user input [13] or as the result of some trajectory optimization problem [15], [16]. Recent work has produced contact-implicit MPC controllers that do not need an explicit contact schedule [17], [18], but these controllers have not yet demonstrated highly dynamic maneuvers on legged robots. Instead, it is common to rely on a prespecified mode sequence and find a trajectory that satisfies the constraints imposed thereby [16], achieving faster solve times but offering no reactivity to unanticipated contact modes. Recent improvements in the speed of contact-implicit trajectory optimization exhibit rapid convergence to solutions in relatively simple numerical settings [19], but their performance on hardware remains unreported.

Fig. 1. Spirit's spatial anchoring controller recovers from a strong rolling disturbance. The resulting perturbation is incurred while engaged in the energetic sagittal plane pitching required by the bounding gait. Despite the high adversarial velocity in roll, the anchoring controller enables the robot to regain its balance and resume stable bounding. The frames shown span approximately 600 ms and offer a visualization of the comparable recovery behaviors quantified in Table I.

A long-established alternative approach to gait planning and control uses low degree-of-freedom dynamical systems (templates) to describe and generate a wide variety of behaviors [20]. Performance arising from these primitives admits strong formal stability guarantees and exhibits significant empirical robustness in the face of parameter mismatch and unmodeled disturbances, as well as substantial departure from formal assumptions [21]. This combination of formal guarantees and robustness has, in turn, enabled highly dynamic behaviors via sequential composition of templates [22]. The resulting locomotion is reliable enough to be used by higher-level planners in mobile manipulation tasks requiring substantial navigation and rearrangement of movable objects [23]. Recent work has examined the idea of automatically generating these compositions at runtime to enable robots to react to their environment [24], [25], with the hope of enabling nearly instantaneous replanning in the event of an unexpected contact event. However, physical applications of this compositional approach to locomotion have historically been restricted to planar behaviors, implemented largely on quadrupeds with almost no actuation authority outside the sagittal plane [21]–[24] to isolate the action of the template,

*This work was supported by AFRL grant FA865015D1845 (subcontract 669737-1) and ONR grant N00014-16-1-2817, a Vannevar Bush Fellowship held by the second author, sponsored by the Basic Research Office of the Assistant Secretary of Defense for Research and Engineering.

The authors are with the GRASP Lab, University of Pennsylvania, Philadelphia, PA 19014. {tmgreco, kod} @ seas.upenn.edu

relying on limited and brittle mechanical compliance of the robot's locked limbs or kinematically unavailable directions to passively stabilize these unactuated out-of-plane degrees of freedom.

To extend these compositional methods to spatial quadrupeds[1], this paper presents an anchoring controller that actively stabilizes the out-of-plane degrees of freedom, enabling the performance of such torso-accelerating sagittal plane behaviors despite substantial out-of-plane disturbances, as shown in Fig. 1. Section II introduces the controller and demonstrates its stability, focusing on its rotational dynamics. Section III presents the empirical results of using this controller to perform a variety of sagittal template-based behaviors in the presence of large out-of-plane disturbances. Section IV concludes with a brief commentary on the significance of these results and directions for future work. An accompanying technical report [27] provides an unabridged account of the calculations in Sections II and III-A.

II. Anchoring Controller

This anchoring controller is designed to admit interoperable parallel composition with any template whose dynamics renders the sagittal plane invariant by imposing almost global attraction down to that submanifold while avoiding any interference with the particular targeted planar subsystem. In this paper, the term *template* denotes a second-order dynamical system on the sagittal plane, which is realized by a set of forces (u_x, u_z) applied at a "virtual toe" in the sagittal plane. (for example, in the experiments of Sec. III, we will be using the sagittal plane controllers presented in [21] and [22].). The anchoring determines a "virtual toe" location in the real world, calculates additional forces and moments necessary for stabilizing the robot's out-of-plane degrees of freedom, and returns toe forces that produce the resulting wrench on the robot.

When two paired legs are in contact with the ground,[2] define the *stance frame* as the right-handed inertial coordinate frame with the $z-$axis pointing up and the $y-$axis pointing from the right toe to the left toe, with the origin at the midpoint between the toes. Define the *body frame* as the right-handed coordinate frame with the $z-$axis normal to the robot's dorsal plane and the $y-$axis pointing from the robot's right hip to its left, with the origin at the robot's center of mass. The term *pose* will denote the transformation in $SE(3)$ that maps the stance frame to the body frame. Define the set $\mathcal{S} \subset SE(3)$ of *sagittal poses* as $\mathcal{S} := \{(p_x, 0, p_z)\} \times \mathcal{P}$, where $\mathcal{P}$ denotes the *pitches* — i.e., the set of rotations around the stance frame that fix the y-axis — and define the *sagittal velocities*, $\mathcal{V} \subset \mathbb{R}^6$, as $\mathcal{V} = \{(\dot{p}_x,\, 0,\, \dot{p}_z,\, 0,\, \alpha,\, 0)\}$. This anchoring controller must make $\mathcal{S} \times \mathcal{V}$ attracting and invariant under the resulting closed loop dynamics.

Assume that the robot behaves as a single rigid body with massless legs, and that two feet are in contact with the ground, either the front feet or the hind feet. Suppose further that the robot's legs do not slip, reach kinematic singularity, or require more torque than the motors can provide.[3] In this configuration, the robot can directly actuate five of the torso's six degrees of freedom. It cannot directly produce a torque about the line between the toes, i.e. in the pitch direction, so this rotational degree of freedom must remain coupled to the x and z translational degrees of freedom. Templates defined in the sagittal plane expect and account for this coupling between x, z, and pitch, so this anchoring controller reserves those degrees of actuation for the template controller. Since the remaining degrees of freedom are fully actuated, the anchoring can use one controller to stabilize the lateral position while a second controller stabilizes the orientation. Let the lateral translation controller take the familiar potential-dissipative form (proportional-derivative, for these translational components of the pose),

$$u_y = -K_p p_y - K_d \dot{p}_y, \tag{1}$$

where u_y is a lateral force applied on the robot at the midpoint of the toes and p_y is the body position in the $y-$direction of the stance frame. If the robot can maintain contact with the ground and if gravity has a negligible effect on the robot's lateral movement, this controller must stabilize the robot's position to the sagittal plane. These assumptions match the observed behavior documented in Section III. Thus, it remains to introduce a controller stabilizing the pitches, $\mathcal{P}$, under the dynamical system on $TSO(3)$:

$$\begin{aligned} \dot{R} &= RJ(\omega)^T \\ \dot{\omega} &= M^{-1}(\tau - \omega \times M\omega),. \end{aligned} \tag{2}$$

This system can also be stabilized by a potential-dissipative controller [28] of the form

$$\tau = -\nabla\Phi(R) - K_D\omega, \tag{3}$$

where the rotation matrix R represents the angular component of the pose, $\omega \in \mathbb{R}^3$ is its angular velocity, and the controller terms are parametrized as

$$K_D = \mathbf{diag}([\kappa_1,\, 0,\, \kappa_2]) \quad \text{and} \quad \Phi(R) = y^T R y \tag{4}$$

for $y = [0,\ 1,\ 0]^T$ and $\kappa_1, \kappa_2 > 0$. The following subsections formally demonstrate that the controller defined in (3) makes $T\mathcal{P} \subset SO(3)$ attracting and invariant.

This demonstration is organized as follows. In Section II-A, calculating the gradient of Φ confirms that $\mathcal{P}$ lies in its critical set, so $T\mathcal{P}$ is an equilibrium of the closed-loop dynamics (2) arising from (3) and thus it is invariant. Section

[1]In this paper, we will call a quadrupedal robot with twelve actuated degrees of freedom a *spatial* quadruped to distinguish its motion from the planar behavior of quadrupeds such as Minitaur [26]. Most quadrupedal robots in the field today are spatial quadrupeds, and this controller can be applied to any of them.

[2]This definition breaks down at some points in behaviors such as the Pronk and Box Jump, during which all four legs are on the ground. The controller defined here could misbehave if the front and back legs define incompatible stance frames, resulting in convergence to neither and internal forces between the toes. In practice, however, the difference between these stance frames was too small to cause any noticeable issues.

[3]These assumptions guarantee feasibility of both the template and anchoring controllers. In practice, these assumptions are frequently violated (e.g. by small amounts of slipping at the toes) without any observed loss of performance, but they are essential for conducting the stability analysis.

II-B continues with the calculation of the Hessian of Φ at the components of its critical set. Section II-C uses total energy as a Lasalle function to show that the critical set of Φ is globally attracting. Section II-D concludes with an examination of the local stability of equilibrium points in each component of the critical set, applying the results from Section II-B to conclude that only point equilibria in $T\mathcal{P}$ are locally attracting, while point equilibria elsewhere in the critical set are unstable. The results of Sections II-C and II-D establish that $T\mathcal{P}$ is "almost globally" attracting in the sense of [28] when the only invariant set generated by the template dynamics in the sagittal plane consists of local equilibrium states. Some of the sagittal template dynamics we use in this work have this property, whereby the combination of global (II-C) and local (II-D) results suffice to guarantee that only a zero measure set of initial conditions generate trajectories that fail to converge to the desired sagittal plane behavior in $T\mathcal{P}$. We conjecture (but do not prove in this paper) that this controller ensures almost global convergence to $T\mathcal{P}$ regardless of the properties of the template dynamics. If this conjecture is sound, as our empirical results suggest, then it formally guarantees global efficacy of this anchoring controller in parallel composition with any desired sagittal-plane behavior (including, for example, the steady state bounding template that introduces a non-equilibrium attracting invariant set) on any spatial quadruped.

A. The Gradient of Φ

Consider the gradient $\nabla_R\Phi$ with respect to $\omega \in \mathbb{R}^3$. Apply equation (3.1) from [29], recalling that $y^T R y = \mathbf{Tr}(yy^T R)$:

$$\nabla_R\Phi(\omega) = \frac{1}{2}\mathbf{Tr}\big((yy^T - R^T yy^T R^T)RJ(\omega)\big), \quad (5)$$

where $J : \mathbb{R}^3 \to \mathfrak{so}(3)$ is the skew map such that $J(a)b = a \times b$. After some massaging, this equation simplifies to

$$\nabla_R\Phi = y \times R^T y. \quad (6)$$

This formulation makes it easy to determine the critical regions of Φ, since $\nabla_R\Phi = 0$ if and only if $R^T y = \lambda y$ for $\lambda \in \{-1, 1\}$. Now $R^T y = y$ if and only if $R \in \mathcal{P}$; hence, it is useful to define the corresponding antipodal set as $\mathcal{Q} := \{R \in SO(3) \mid R^T y = -y\}$. These two disjoint sets comprise the critical set of Φ. Since for any $(R, \omega) \in T\mathcal{P}$, R is in the critical set of Φ and ω is in the null space of K_D, so the controller defined in (3) exerts zero input, and thus $T\mathcal{P}$ is invariant under this controller. Fig. 2 shows what configurations in $\mathcal{P}$ and $\mathcal{Q}$ actually look like for the robot.

B. The Hessian of Φ

Lemma 3.2 from [29] gives an expression for the Hessian of Φ at any critical point as a symmetric bilinear form on $\mathfrak{so}(n)$. Applying this result to (4) yields

$$h_\Phi(U, V) = -\mathbf{Tr}(yy^T RUV) \quad (7)$$

where $U, V \in \mathfrak{so}(3)$. To determine the relative maxima and minima of Φ, evaluate the Hessian for some $U = V$. Since $\mathfrak{so}(3)$ is isomorphic to $\mathbb{R}^3$, there is some u such that

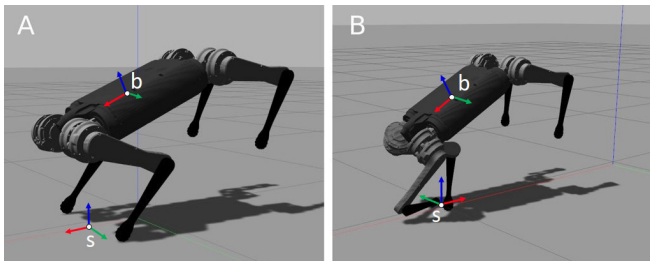

Fig. 2. Visualizing the critical set of Φ. A displays a pose is in $\mathcal{P}$, and B displays a pose in $\mathcal{Q}$. This latter configuration is kinematically feasible but difficult to achieve. In each picture, the stance frame is labeled 's' and the body frame 'b'.

$J(u) = U$. To simplify evaluation, apply this isomorphism to represent the Hessian as a quadratic form on $\mathbb{R}^3$, obtaining the Hessian matrix:

$$H_\Phi(R) := J(y)^T J(R^T y). \quad (8)$$

If R is in the critical set, $H_\Phi(R) = \lambda J(y)^T J(y)$. Evaluating this equation for $R \in \mathcal{P}$,

$$H_\Phi(R) = \begin{bmatrix} 1 & 0 & 0 \\ 0 & 0 & 0 \\ 0 & 0 & 1 \end{bmatrix} =: H_\mathcal{P}. \quad (9)$$

Similarly, for $R \in \mathcal{Q}$,

$$H_\Phi(R) = \begin{bmatrix} -1 & 0 & 0 \\ 0 & 0 & 0 \\ 0 & 0 & -1 \end{bmatrix} =: H_\mathcal{Q}. \quad (10)$$

Thus $\mathcal{P}$ is a minimum and $\mathcal{Q}$ a maximum of Φ on $SO(3)$, and since $SO(3)$ has no boundary, these extrema are global. The vector y spans both the kernel of these Hessian matrices and the tangent spaces of both $\mathcal{P}$ and $\mathcal{Q}$, and thus Φ is a Morse-Bott function on $SO(3)$ [30].

C. Φ as a potential

The dynamical system defined in (2), with τ is defined as in (3), describes the effect of the orientation controller on the robot in the absence of any other torques. Define the stance-frame moment of inertia $M(R) = R^T I_B R$, where I_B denotes the diagonal matrix that expresses the robot's inertia tensor in the body frame. Consider the total energy function $\eta : TSO(3) \to \mathbb{R}$ defined as

$$\eta(R, \omega) = \Phi(R) + \frac{1}{2}\omega^T M(R)\omega, \quad (11)$$

where ω is the robot's angular velocity in the stance frame. This function is a Lasalle function for the system defined in (2) [31], [32]. Note that $\eta(R, \omega) \geq 0$, since $\Phi(R) \geq 0$ and M is symmetric positive definite. Examining $\dot{\eta}(R, \omega)$,

$$\dot{\eta}(R, \omega) = \omega^T(y \times R^T y) + \omega^T M\dot{\omega} + \frac{1}{2}\omega^T \dot{M}\omega. \quad (12)$$

Since $M = R^T I_B R$,

$$\omega^T \dot{M}\omega = 2\omega^T \dot{R}^T I_B R\omega = 2\omega^T(\omega \times M\omega) = 0. \quad (13)$$

Substitute (3), (13), and (2) into (12) and apply (6):

$$\dot{\eta}(R, \omega) = -\omega^T K_D \omega, \quad (14)$$

and since K_D is positive semidefinite, $\dot{\eta} \leq 0$. Note that $\dot{\eta} = 0$ if and only if $\omega \in \mathrm{span}(y)$ in the stance frame.

By Lasalle's invariance principle, the largest invariant subset of $\eta^{-1}[0]$ is attracting and contains all forward limit points of this dynamical system; it remains to be shown whether this subset contains $T\mathcal{P}$. Let $\mathcal{L} \subset \eta^{-1}[0]$ be this largest invariant subset. For any $(R, \omega) \in \mathcal{L}$, the angular acceleration must be in the y direction to remain in that set under the flow of 2. If $\omega = \alpha y$ for some $\alpha \in \mathbb{R}$, then

$$\begin{aligned} \dot{\alpha} y &= \dot{\omega} \\ &= M^{-1}\big(-\nabla\Phi(R) - K_D(\alpha y) - (\alpha y) \times M(\alpha y)\big) \\ \dot{\alpha} M y &= -(y \times R^T y) - \alpha^2 y \times My. \end{aligned} \tag{15}$$

Since M is symmetric positive definite, My must have a nonzero component in the y direction. However, neither of the terms on the RHS of (15) can have any nonzero component in the y direction, so (15) can only hold if $\dot{\alpha} = 0$, from which it follows that

$$0 = -(y \times R^T y) - \alpha^2 y \times My. \tag{16}$$

To completely characterize the rotational trajectories $\big(R(t), \omega(t)\big)$ of the flow generated by (2) that satisfy (16), it is helpful to impose the consequent necessary requirement that time variation of (16) also evaluate to the constant 0. Taking the derivative of (16) with respect to time yields

$$\begin{aligned} 0 &= -y \times R(\alpha y \times y) - 2\alpha\dot{\alpha} y \times My - \alpha^2\big(y \times (\alpha y \times My) \\ &\quad + y \times M(\alpha y \times y)\big) \\ 0 &= -\alpha^3\big(y \times (y \times My)\big). \end{aligned} \tag{17}$$

Since y must be perpendicular to $y \times My$ if the latter is nonzero, (17) can only be satisfied if $\alpha = 0$ or $y \times My = 0$. In either case, (16) simplifies to

$$0 = -y \times R^T y = -\nabla\Phi(R). \tag{18}$$

Thus $(R, \omega) \in \mathcal{L}$ if and only if $R \in \mathcal{P} \cup \mathcal{Q}$ and $\omega \in \mathrm{span}(y)$. The embeddings in $\mathbb{R}^3$ of the tangent spaces of both $\mathcal{P}$ and $\mathcal{Q}$ are both represented by $\mathrm{span}(y)$ in the stance frame, so $\mathcal{L} = T\mathcal{P} \cup T\mathcal{Q}$. By Lasalle's invariance principle [31], [32], $T\mathcal{P} \cup T\mathcal{Q}$ is attracting and contains all forward limit points.

D. Local Stability of Equilibria

Suppose that, in addition to the anchorning controller (3), the robot is subject to some template dynamics on $T\mathcal{P}$; further suppose that the template is "pitch-steady" as described in [33], so there will be some $p_0 \in \mathcal{P}$ that is locally attracting within $T\mathcal{P}$. The template dynamics around p_0 in $T\mathcal{P}$ can be approximated by a second-order linear system

$$\begin{bmatrix} \dot{p} \\ \ddot{p} \end{bmatrix} = \begin{bmatrix} 0 & 1 \\ -\frac{\gamma}{\mu} & -\frac{\beta}{\mu} \end{bmatrix} \begin{bmatrix} p \\ \dot{p} \end{bmatrix}, \tag{19}$$

where β, γ, and μ are positive constants. Since $T\mathcal{P}$ is invariant under (3), the anchoring will not alter this behavior, and the linearized dynamics about p_0 in $TSO(3)$ are

$$\begin{bmatrix} \dot{\theta} \\ \dot{\omega} \end{bmatrix} = \begin{bmatrix} 0 & I \\ -M^{-1}(H_{\mathcal{P}} + K) & -M^{-1}(K_D + B) \end{bmatrix} \begin{bmatrix} \theta \\ \omega \end{bmatrix}, \tag{20}$$

where $K = \mathbf{diag}([0, \gamma, 0])$ and $B = \mathbf{diag}([0, \beta, 0])$. Since $K_D + B$ and M are symmetric positive definite, and $H_{\mathcal{P}} + K$ is positive definite, (20) is asymptotically stable [28, Lemma 3.5]. Thus p_0 is an attractor.

Conversely, consider the action of the same template dynamics when the robot's pose and velocity lie in $T\mathcal{Q}$. There will be some corresponding equilibrium point $q_0 \in \mathcal{Q}$ which admits the same linearized dynamics as in (19). In this case, the linearized dynamics about q_0 on $TSO(3)$ are

$$\begin{bmatrix} \dot{\theta} \\ \dot{\omega} \end{bmatrix} = \begin{bmatrix} 0 & I \\ -M^{-1}(H_{\mathcal{Q}} + K) & -M^{-1}(K_D + B) \end{bmatrix} \begin{bmatrix} \theta \\ \omega \end{bmatrix}. \tag{21}$$

In this system, $H_{\mathcal{Q}} + K$ has both positive and negative eigenvalues so q_0 is a saddle [28, Lemma 3.5].

These local stability results clarify the results of the previous section. The equilibrium point of any pitch-stable template is stable in $\mathcal{P}$ but unstable in $\mathcal{Q}$, suggesting that of the two disjoint sets that compose a global attractor on $SO(3)$, only $\mathcal{P}$ is locally attracting. While the extension of this result to limit cycles or abitrary trajectories in pitch remains unproven, the following empirical results support the plausibility of such a conjecture.

III. Experimental Results

A. Implementation Details

The implementation of this controller on a Ghost Spirit [34] uses a hierarchical structure to emphasize the compositional nature of this framework. Each of the three layers is defined as a separate C++ object. At the highest layer, *behavior* objects govern the sequential or parallel composition of template objects, passing them high-level inputs and handling transitions between them. The *template* objects make a sagittal-plane approximation of the robot's dynamics and output appropriate planar forces. The *anchoring* object takes these forces and calculates forces for each toe to exert in 3D space so that the robot's dynamics in the sagittal plane match the template dynamics and the out-of-plane dynamics are governed by the controller defined in (1) and (3).

The anchoring controller calculates these toe forces as follows. Let (u_x, u_z) be the template forces and (u_y, τ) the outputs of (1) and (3) respectively. Let r be the vector from the robot's center of mass to the midpoint between the toes, and let k be the vector between the midpoint of the toes and the left toe. Consider the action of the toe forces on the body represented in sum and difference coordinates, where s is the sum of the toe forces and d is their difference. In these coordinates, the net force acting on the body is s, and the net torque is $r \times s + k \times d$. Set $s = [u_x, u_y, u_z]^T$. The term $r \times s$ is the only torque acting on pitch, since pitches are rotations around k. Its action in the yaw and roll directions is negligible in practice, although a term could be added to τ to cancel it. The force d is calculated by $d = J(k)^\dagger \tau$, where $J(k)$ is a skew-symmetric matrix as defined in Section II-A, and $J(k)^\dagger$ is its pseudoinverse.[4] Having calculated s and d

[4]Nothing is lost by restricting d to the image of $J(k)^\dagger$. Recall that k points in the direction between the toes; any component of d pointing in that direction would generate no torque on the system.

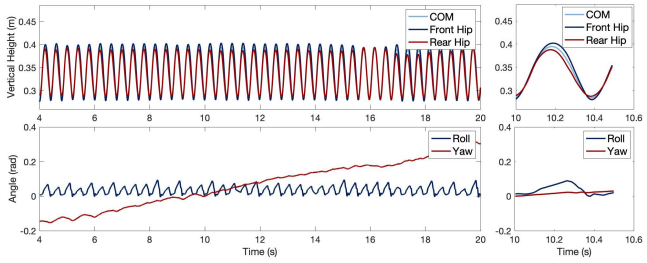

Fig. 3. The hip heights, COM height, roll, and yaw of Spirit during feedback-stabilized pronking. Plots on the right focus on a typical single period of the gait. Note that the yaw (and all traces displayed) are plotted with respect to a fixed world frame, not each stance frame. See Section III-B.1 for an explanation of the gradual drift in yaw.

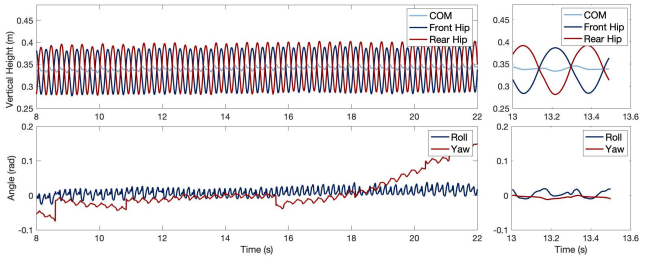

Fig. 4. The hip heights, COM height, roll, and yaw of Spirit during preflexively stable bounding. Plots on the right focus on a typical single period of the gait. Note that the yaw (and all traces displayed) are plotted with respect to a fixed world frame, not each stance frame. See Section III-B.1 for an explanation of the gradual drift in yaw.

in terms of u_x, u_y, u_z, and τ, the anchoring inverts the sum and difference transformation to obtain the forces at each toe [27], and the Ghost SDK calculates the corresponding joint torques [35].

All of the behaviors discussed in the next sections used the exact same implementation of the anchoring controller (1, 3). Relying on the same fixed gains throughout all the experiments reported here, it needed no further tuning to suit specific template compositions. Furthermore, the template and behavior layers are the same controllers used with Minitaur [21], [22], although updates to the Ghost SDK made it impossible to directly reuse the code from Minitaur.

B. Dynamic Gaits

1) Steady-State Performance: The anchoring controller of Sec. II (1, 3) enabled Spirit to replicate the feedback-stabilized pronk and preflexively-stable bound described in [21]. The resulting behaviors were recorded using a Vicon motion tracking system. Figs. 3 and 4 show data from the Vicon system and the robot's internal IMU. The sagittal plane motion of the robot, plotted in the top portion of each figure, exhibits the expected behavior: hips move in phase with each other when pronking and out of phase when bounding. Even though the anchoring controller can only act during isolated stance periods (approximately 150 ms out of the roughly 350 ms stride period), it stabilizes both yaw and roll during that time. In the bottom-right plots of both figures, note that most of the deviation in roll takes place when neither hip is near the bottom, i.e. during the aerial phase when the anchoring controller has no physical affordance. The drift in yaw that both gaits display is not unexpected since the stance frame changes at each touchdown. The robot cannot control its yaw during flight and it lands in a new stance frame for which the current yaw is close to zero. An additional lateral force at the toe could stabilize the robot to some desired heading in the world frame, but such a hybrid discrete event controller would fall outside the scope of this paper.

2) Disturbance Rejection: Using this anchoring, Spirit exhibited considerable robustness to out-of-plane disturbances during these steady-state gaits. These disturbances took two forms. Lateral force disturbances were imparted via pulls on a string attached near the robot's center of mass, and disturbances in yaw torque were induced by pulls on a string attached approximately one body length (45 cm) from the

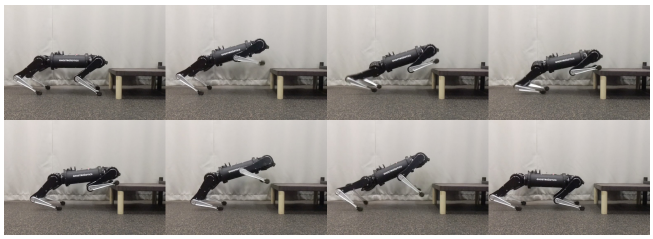

Fig. 5. Spirit performing the mount and dismount behaviors from [22].

robot's center of mass. Table I summarizes the results of these trials. The *baseline* for each gait is the peak velocity value measured in each direction during the unperturbed trials shown in Figs. 3 and 4. Each trial is considered a *pass* if the robot recovers from the disturbance and resumes normal gait execution, a *gait failure* if the robot rejects the disturbance but is unable to resume the gait, or an *anchoring failure* if the disturbance causes the robot to fail in some out-of-plane degree of freedom. These results show repeatable successful rejection of disturbances that increased the velocity, exhibiting an 80% recovery rate from lateral velocities up to twice the maximum encountered during the unperturbed gait. These results corroborate the robustness of the template controllers reported in [21], [22], [33] and suggesting an ample basin of attraction for the new anchoring controller (1, 3). The accompanying video includes footage of some of these trials [36].

The trials exhibited two distinct gait failure modes. In the first and more common mode, the disturbance interfered with the controller that governs the gait's fore-aft velocity (based on [37] and not formally treated elsewhere). The robot would accelerate forward and fail to control its velocity. The second template failure mode caused ringing in the phase-coupling controller for the pronk, resulting in a very high-frequency bound. The anchoring failures were much more dramatic: the robot would lose its balance and roll onto its back.

These failure modes did not always exhibit a clear correlation with the magnitude of the induced change in velocity. For example, the lateral disturbances that caused the gait failures for the bound each generated a change in lateral velocity of approximately 0.38 m/s, but the robot also successfully withstood a disturbance that caused a change in velocity of 0.63 m/s while bounding.

C. Transitional Maneuvers

TABLE I

RECOVERY OF STEADY-STATE GAITS FROM TORSO VELOCITY PERTURBATIONS

Gait	Disturbance	Baseline	Perturbation Velocity Range	Perturbation to Baseline Ratio	Pass Rate	Gait Failure	Anchoring Failure
Bound	Lateral	0.075 m/s	0.28 - 0.63 m/s	3.7 - 8.4	10/12	2/12	0/12
Bound	Yaw	0.4 rad/s	1 - 3 rad/s	2.5 - 7.5	18/21	3/21	0/21
Pronk	Lateral	0.15 m/s	0.25 - 0.32 m/s	1.6 - 2.1	11/13	2/13	0/13
Pronk	Lateral	0.15 m/s	0.32 - 0.85 m/s	2.1 - 5.6	8/13	4/13	1/13
Pronk	Yaw	0.45 rad/s	1 - 1.8 rad/s	2.2 - 4	8/10	2/10	0/10
Pronk	Yaw	0.45 rad/s	1.8 - 3 rad/s	4 - 6.6	5/10	5/10	0/10

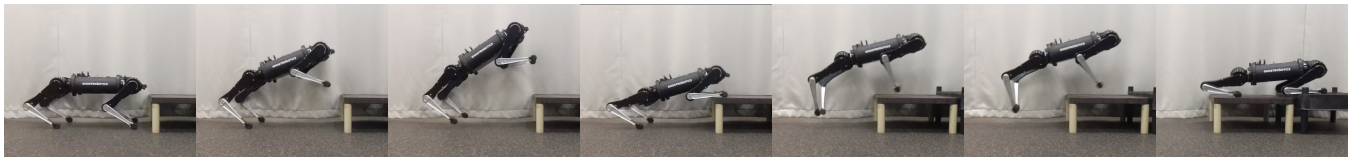

Fig. 6. Snapshots of Spirit performing the box-jump behavior from [22].

TABLE II

RESULTS OF TRANSITIONAL BEHAVIORS WITH YAW DISTURBANCES

Behavior	Disturbance	Success Rate	Peak Yaw Velocity
Mount	0.05 rad	5/5	0.73 $\pm$0.15 rad/s
Mount	0.15 rad	4/5	0.72 $\pm$0.13 rad/s
Boxjump	0.05 rad	5/5	1.09 $\pm$0.52 rad/s
Boxjump	0.15 rad	4/5	1.22 $\pm$0.10 rad/s

1) Performance: Spirit also used this anchoring to execute the mount, dismount, and box-jump defined in [22]. Snapshots of the mount and dismount are presented in Fig. 5, and of the box-jump behavior in Fig. 6. Spirit successfully performed each behavior repeatedly five times out of five attempts, meeting the same measure of repeatability as in [22]. Despite these behaviors' short stance phases and high-velocity flight phases, the anchoring reliably stabilized the out-of-plane motion of the robot.

2) Disturbance Rejection: When the Mount and Boxjump behaviors from [22] were executed from initial conditions that included displacements in yaw between the body frame and the stance frame, the anchoring was able to reject these disturbances. In these initial conditions, the robot was positioned with its rear toes in the same location relative to the box as in the undisturbed trials, but the body was rotated with respect to the toes by some specified angle. Each behavior was tested at nominal displacements of 0.05 and 0.15 radians, with five trials at each initial condition.

Table II shows the results of these trials. Trials were classified as a success if the robot ended up in the behavior's desired state. For the mount, this meant having its front legs on the box and its hind legs on the ground, and for the boxjump, this meant standing with all four feet on top of the box. The peak yaw velocity is the magnitude of the largest yaw velocity measured by the robot's IMU during the execution of the behavior; the table shows the mean and standard deviation of this value for each set of trials. Small displacements caused significant yawing motion during the behavior but did not cause any failures. As the displacements grew, so did their effects on the robot's dynamics during the behavior, causing the pass rate to drop to 80%. The accompanying video presents several successful trials [36].

IV. CONCLUSION

This paper presents a controller that anchors sagittal plane templates in a spatial quadruped by applying a potential dissipative controller [28] whose global minimum comprises a sagittal copy of $TSE(2)$ considered as a submanifold of the spatial body's full six degree of freedom state space, $TSE(3)$. The formal properties of this controller guarantee stability in the stance mode dynamics assuming a pair of sticking toes, and the empirical results show strong enough performance during short stance phases of approximately 100-200ms to recover from significant out-of-plane perturbations without interfering with the template dynamics. Since each component of the modular behaviors used in this paper admits formal analysis, it is possible to reason in advance about their action when composed together. In consequence, the behaviors reported in this paper incorporate algorithms identical to those introduced in [21] and [22]. Their software implementation is almost entirely hardware agnostic: these behaviors can be tuned to run on any robot with adequate affordance and traction. These results demonstrate the robust portability of provably interoperable modular control components across a variety of hardware platforms and behaviors.

It bears noting that while this anchoring was designed with compositionally-defined controllers in mind, it could be applied to stabilize any sagittal-plane controller. The ability to reliably use a sagittal-plane model for MPC would greatly increase the rate at which such a controller would run.

Work in progress employs this anchoring and the behaviors reported in Section III-C for mobile manipulation, extending the work in [23]. Spirit's additional degrees of freedom offer a greater variety of ways to interact with obstacles, which could lead to the execution of more complex tasks in more tightly-constrained environments. In particular, if such a hybrid controller could be synthesized with the mode-reactive template behaviors presented in [24], [33], then recovery from misjudged environment geometries and substrate mechanics would be possible in realtime.

ACKNOWLEDGMENTS

Matthew Kvalheim and J. Diego Caporale helped refine the arguments in Section II. Maeve Juday helped with editing.

REFERENCES

[1] A. M. Johnson, M. T. Hale, G. C. Haynes, and D. E. Koditschek, "Autonomous legged hill and stairwell ascent," in *2011 IEEE International Symposium on Safety, Security, and Rescue Robotics*, pp. 134–142, 2011.

[2] T. Miki, J. Lee, J. Hwangbo, L. Wellhausen, V. Koltun, and M. Hutter, "Learning robust perceptive locomotion for quadrupedal robots in the wild," *Science Robotics*, vol. 7, no. 62, p. eabk2822, 2022.

[3] M. Hutter, "Legged robots on the way from subterranean," in *Robotics and Automation (ICRA), 2022 IEEE International Conference on*, IEEE, 2022. Keynote address.

[4] L. Clemente, O. Villarreal, A. Bratta, M. Focchi, V. Barasuol, G. Muscolo, and C. Semini, "Foothold evaluation criterion for dynamic transition feasibility for quadruped robots," in *IEEE International Conference on Robotics and Automation (ICRA)*, 2022.

[5] A. Kumar, Z. Fu, D. Pathak, and J. Malik, "Rma: Rapid motor adaptation for legged robots," in *Robotics: Science and Systems*, 2021.

[6] D. Esteban, O. Villarreal, S. Fahmi, C. Semini, and V. Barasuol, "On the Influence of Body Velocity in Foothold Adaptation for Dynamic Legged Locomotion via CNNs," in *International Conference on Climbing and Walking Robots (CLAWAR)*, (Moscow, Russia), pp. 353–360, Aug. 2020.

[7] G. B. Margolis, G. Yang, K. Paigwar, T. Chen, and P. Agrawal, "Rapid locomotion via reinforcement learning," in *Robotics: Science and Systems*, 2022.

[8] N. Rudin, D. Hoeller, M. Bjelonic, and M. Hutter, "Advanced skills by learning locomotion and local navigation end-to-end," in *2022 IEEE/RSJ International Conference on Intelligent Robots and Systems (IROS)*, pp. 2497–2503, 2022.

[9] G. Bellegarda and Q. Nguyen, "Robust quadruped jumping via deep reinforcement learning," 2020. Available at `https://arxiv.org/abs/2011.07089`.

[10] A. Iscen, G. Yu, A. Escontrela, D. Jain, J. Tan, and K. Caluwaerts, "Learning agile locomotion skills with a mentor," in *Proceedings - IEEE International Conference on Robotics and Automation*, vol. 2021-May, pp. 2019–2025, 2021.

[11] J. Di Carlo, P. M. Wensing, B. Katz, G. Bledt, and S. Kim, "Dynamic locomotion in the mit cheetah 3 through convex model-predictive control," in *2018 IEEE/RSJ International Conference on Intelligent Robots and Systems (IROS)*, pp. 1–9, 2018.

[12] F. Farshidian, E. Jelavic, A. Satapathy, M. Giftthaler, and J. Buchli, "Real-time motion planning of legged robots: A model predictive control approach," *CoRR*, vol. abs/1710.04029, 2017.

[13] D. Kim, J. D. Carlo, B. Katz, G. Bledt, and S. Kim, "Highly dynamic quadruped locomotion via whole-body impulse control and model predictive control," *CoRR*, vol. abs/1909.06586, 2019.

[14] L. Righetti and S. Schaal, "Quadratic programming for inverse dynamics with optimal distribution of contact forces," in *2012 12th IEEE-RAS International Conference on Humanoid Robots (Humanoids 2012)*, pp. 538–543, 2012.

[15] H. Park, P. M. Wensing, and S. Kim, "Online planning for autonomous running jumps over obstacles in high-speed quadrupeds," in *Robotics: Science and Systems*, vol. 11, 2015.

[16] M. Chignoli and S. Kim, "Online trajectory optimization for dynamic aerial motions of a quadruped robot," in *Proceedings - IEEE International Conference on Robotics and Automation*, vol. 2021-May, pp. 7693–7699, 2021.

[17] S. L. Cleac'h, T. A. Howell, M. Schwager, and Z. Manchester, "Linear contact-implicit model-predictive control," *CoRR*, vol. abs/2107.05616, 2021.

[18] A. Aydinoglu and M. Posa, "Real-time multi-contact model predictive control via ADMM," *CoRR*, vol. abs/2109.07076, 2021.

[19] S. Tonneau, D. Song, P. Fernbach, N. Mansard, M. Taïx, and A. D. Prete, "SL1M: sparse l1-norm minimization for contact planning on uneven terrain," *CoRR*, vol. abs/1909.09044, 2019.

[20] R. J. Full and D. E. Koditschek, "Templates and anchors: Neuromechanical hypotheses of legged locomotion on land," *Journal of Experimental Biology*, vol. 202, no. 23, pp. 3325–3332, 1999.

[21] A. De and D. E. Koditschek, "Vertical hopper compositions for preflexive and feedback-stabilized quadrupedal bounding, pacing, pronking, and trotting," *The International Journal of Robotics Research*, vol. 37, no. 7, pp. 743–778, 2018.

[22] T. T. Topping, V. Vasilopoulos, A. De, and D. E. Koditschek, "Composition of templates for transitional pedipulation behaviors," in *Robotics Research* (T. Asfour, E. Yoshida, J. Park, H. Christensen, and O. Khatib, eds.), Springer Proceedings in Advanced Robotics, (Cham), p. 626–641, Springer International Publishing, 2022.

[23] V. Vasilopoulos, T. T. Topping, W. Vega-Brown, N. Roy, and D. E. Koditschek, "Sensor-Based Reactive Execution of Symbolic Rearrangement Plans by a Legged Mobile Manipulator," in *IEEE/RSJ International Conference on Intelligent Robots and Systems*, pp. 3298–3305, 2018.

[24] T. T. Topping and D. E. Koditschek, "A palette of sagittal plane template compositions toward reactive transitional legged robot behaviors." Fifth Workshop Towards Real World Deployment of Legged Robots, Jun 2021. Available at `https://www.youtube.com/watch?v=tDWtWMqZckg`.

[25] Y. Zhao, Y. Li, L. Sentis, U. Topcu, and J. Liu, "Reactive task and motion planning for robust whole-body dynamic locomotion in constrained environments," *The International Journal of Robotics Research*, vol. 41, no. 8, pp. 812–847, 2022.

[26] G. Kenneally, A. De, and D. E. Koditschek, "Design principles for a family of direct-drive legged robots," *IEEE Robotics and Automation Letters*, vol. 1, pp. 900–907, July 2016.

[27] T. Greco and D. E. Koditschek, "Technical report on: Anchoring sagittal plane templates in a spatial quadruped," 2022. Available at `https://arxiv.org/abs/2209.15617`.

[28] D. E. Koditschek, "The application of total energy as a lyapunov function for mechanical control systems," *Contemporary Mathematics*, February 1989.

[29] H. Bozma, W. Gillam, and F. Öztürk, "Morse-bott functions on orthogonal groups," *Topology and its Applications*, vol. 265, p. 106807, 2019.

[30] R. Bott, "Nondegenerate critical manifolds," *Annals of Mathematics*, vol. 60, no. 2, pp. 248–261, 1954.

[31] J. LaSalle, "Some extensions of liapunov's second method," *IRE Transactions on Circuit Theory*, vol. 7, no. 4, pp. 520–527, 1960.

[32] H. Khalil, *Nonlinear Systems*. Pearson Education, Prentice Hall, 2002.

[33] A. De, T. T. Topping, J. D. Caporale, and D. E. Koditschek, "Mode-reactive template-based control in planar legged robots," *IEEE Access*, vol. 10, pp. 16010–16027, 2022.

[34] Ghost Robotics, "Spirit 40." `https://www.ghostrobotics.io`.

[35] Ghost Robotics, "Ghost robotics sdk documentation." `https://ghostusers.gitlab.io/docs/index.html`.

[36] "Anchoring sagittal plane templates in a spatial quadruped." [Online]. Available: `https://youtu.be/SejLt0Hx2uQ`.

[37] M. Raibert, *Legged Robots that Balance*. Artificial Intelligence, MIT Press, 1986.